Chemico-Biological Interactions 418 (2025) 111609

Contents lists available at ScienceDirect

Chemico-Biological Interactions

journal homepage: www.elsevier.com/locate/chembioint

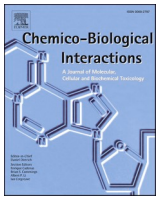

Research paper

Fluorescent substrates enable specific detection and structure-function insights into human aldehyde dehydrogenase isoforms

Raquel Pequerul [a,*], Daniela Covaleda [a], Andrés S. Sánchez-Vaca [a], Laura Torres [a], Andrada Constantinescu [b], Mileidys Perez-Alea [b], Xavier Parés [a], Jaume Farrés [a,**]

[a] Department of Biochemistry and Molecular Biology, Faculty of Biosciences, Universitat Autònoma de Barcelona, Bellaterra, Cerdanyola del Vallès, Barcelona, 08193, Spain

[b] Unit of Research in Cellular and Molecular Biology, Advanced BioDesign-ABD, Saint Priest, France

ARTICLE INFO

Keywords:
Breast cancer
Enzyme inhibition
Fluorescence
Kinetic properties
Oxidoreductases
Structure-function relationships

ABSTRACT

Aldehyde dehydrogenase (ALDH) isoforms are widely used as biomarkers and potential drug targets in cancer research. Quantitation of ALDH enzymatic activity in biological samples often relies on the use of commercially available assays that are quite unspecific and do not discriminate between the various ALDH isoforms. The availability of highly purified recombinant ALDH isoforms allowed us to perform a full kinetic characterization of ALDH isoforms with fluorogenic substrates, BODIPY™-aminoacetaldehyde (BAAA), the ALDEFLUOR™ assay reagent, and two naphthaldedyde derivatives, 6-methoxy-2-naphthaldehyde (MONAL-62) and 7-methoxy-1-naphthaldehyde (MONAL-71). All ALDH1A isoforms were active to different extend with BAAA, while ALDH3A1 did not show any activity. Remarkable kinetic differences between ALDH1A1, ALDH1A2, ALDH1A3, ALDH2 and ALDH3A1 were observed with naphthaldehyde derivatives. Exquisite sensitivity was attained with MONAL-62 with a lower detection limit of 2 amol or 10^6 molecules of enzyme per microliter for ALDH1A1. The high substrate specificity of ALDH1A1 for MONAL-71 provides an alternative assay for the unambiguous identification of this isoform. Enzymatic properties of isoforms were accounted for by *in silico* simulations of substrate docking to the active site of ALDH structures. In addition to substrate specificity, inhibitor selectivity of each isoform, as assessed by incubation with DIMATE and ABD0171 inhibitors, provided additional information about isoform composition in low-activity samples isolated from cell extracts. The method was successfully applied to the detection of ALDH isoform activity in triple-negative breast cancer cells.

1. Introduction

The aldehyde dehydrogenase (ALDH) superfamily is encoded by 19 genes in the human genome, each producing isoforms characterized by different oligomeric structures, substrate specificities, biological roles, tissue expression and subcellular localization. ALDH catalyzes the irreversible $NAD(P)^+$-dependent oxidation of aldehydes to their corresponding carboxylic acids, playing critical roles in detoxifying reactive aldehydes and protecting cells against oxidative stress. Physiological substrates include carbonyl compounds derived from hormones, lipid peroxidation products, amino acid and neurotransmitter intermediates. Relevantly, allelic variants of ALDH have been associated with various disease conditions, alongside epigenetic and transcriptional changes affecting their expression levels. The ALDH1A subfamily members, ALDH1A1, ALDH1A2 and ALDH1A3, participate in the conversion of retinaldehyde to retinoic acid [1], pivotal for embryonic development, epithelia maintenance, immunomodulation and cancer [2]. ALDH2, closely related to ALDH1A, primarily metabolizes ethanol-derived acetaldehyde while ALDH3A1 is abundant in corneal tissue with a protecting role against lipid peroxidation and UV radiation. These isoforms have attracted significant attention due to their frequent upregulation in various cancer types, including cancer stem cells, and their

Abbreviations: ABD0171, S-methyl 4-[dimethyl(2-{2,4-dimethylphenoxy}ethyl)amino]-4-methylpent-2-ynethioate; ALDH, aldehyde dehydrogenase; ALDH1A1, aldehyde dehydrogenase family 1 member A1; BAAA, BODIPY™-aminoacetaldehyde; DIMATE, S-methyl 4-(dimethylamino)-4-methylpent-2-ynethioate; MONAL-62, 6-methoxy-2-naphthaldehyde; MONAL-71, 7-methoxy-1-naphthaldehyde; RMSD, root-mean-square deviation.

* Corresponding author.
** Corresponding author.
E-mail addresses: raquel.pequerul@uab.cat (R. Pequerul), jaume.farres@uab.cat (J. Farrés).

https://doi.org/10.1016/j.cbi.2025.111609
Received 29 April 2025; Received in revised form 12 June 2025; Accepted 17 June 2025
Available online 18 June 2025

implication in tumor chemoresistance, metastasis and recurrence, making them prominent candidates in drug targeting efforts [3,4].

Assessing ALDH enzymatic activity is fundamental for understanding its functional implications in biological processes and disease contexts. ALDH activity can be measured fluorometrically *in vitro* and in intact cells by using various fluorescent substrates (Table S1). These fluorescent molecules offer exceptional sensitivity, enabling measurement and visualization of ALDH activity across enzymatic assays, cell and tissue extracts, flow cytometry, confocal microscopy and high-throughput screening. For instance, the oxidation activity of ALDH in isolated enzyme preparations is typically determined by monitoring the increase in NAD(P)H fluorescence [5].

Naphthalene derivatives, such as 6-methoxy-2-naphthaldehyde (MONAL-62) and 7-methoxy-1-naphthaldehyde (MONAL-71), are suitable substrates for detecting ALDH1 isoforms in assays involving cell and tissue extracts. These substrates were initially introduced by Wierzchowski and collaborators [6] for measuring ALDH activity in human blood, saliva, and organ biopsy samples. Since then, MONAL-62 and MONAL-71 have served as fluorescent substrates to monitor ALDH activity in serum and tissue samples from cancer patients[7–12]. These substrates exhibit intense fluorescence spectra that do not overlap with that of typical proteins or that of NADH (Fig. S1), making them suitable for detecting ALDH even in samples with low activity, despite some noted limitations dealing with hemolysis and artifactual fluorescent complexes in plasma/serum samples or the lack of appropriate controls [13]. However, a comprehensive kinetic characterization of each ALDH isoform with these substrates is still needed.

In intact cells, the method of choice to detect ALDH activity is the ALDEFLUOR™ assay [14]. This technique uses BODIPY-aminoacetaldehyde (BAAA) as a substrate and has been widely employed to detect ALDH activity by flow cytometry, particularly for identifying cancer stem cells. However, the assay lacks ALDH-isoform specificity, which complicates data interpretation[15–17]. Several alternative probes have been also developed, including AlDeSense [18], AldeRed 588-A, a red-shifted fluorescent substrate [19,20], Amino BODIPY-Based Blue Fluorescent Probes [21,22], Near-infrared (NIR) fluorescent probes [23–26], and a fluorogenic isatin-naphthalimide ALDH1A1 inhibitor [27]. Some of these approaches require using the pan-ALDH inhibitor 4-diethylaminobenzaldehyde (DEAB) and blocking cellular efflux transporters to retain the fluorescent reaction product intracellularly [28].

Comprehensive kinetic data for ALDH isoforms with MONAL and ALDEFLUOR™ substrates have been lacking, precluding unambiguous interpretations of enzymatic activity in complex biological samples. Another shortcoming has been the urgent need for sensitive detecting tools and robust experimental protocols to isolate the contributions of specific ALDH isoforms in heterogeneous populations like cancer stem cells.

In the present work, the availability of purified active ALDH isoforms (ALDH1A1, ALDH1A2, ALDH1A3, ALDH2 and ALDH3A1) [5] has enabled a comprehensive kinetic characterization using BODIPY-aminoacetaldehyde, MONAL-62 and MONAL-71, along with comparison to the standard hexanal substrate. Molecular docking simulations have been used to rationalize the experimental data in terms of structure-activity relationships. The use of these naphthalene derivatives has resulted in a significantly enhanced sensitivity for *in vitro* assays, particularly with low-activity samples from cell extracts. Finally, the combined use of activity determination with naphthalene derivatives and the inhibition with DIMATE and ABD0171 has facilitated the identification and quantification of single ALDH isoforms, especially ALDH1A1.

2. Materials and methods

2.1. ALDH substrates and inhibitors

BODIPY™ (4,4-difluoro-5,7-dimethyl-4-bora-3a,4a-diaza-*s*-indacene)-aminoacetaldehyde diethyl acetal (BAAA-DA) was generously provided by STEMCELL Technologies SARL (France) and served as the fluorescent substrate for measuring ALDH activity *in vitro*. MONAL-62 and MONAL-71, fluorescent naphthalene derivatives were purchased from Cymit Quimica and used to detect ALDH activity in cell extracts. Hexanal was obtained from Sigma-Merck and utilized as a standard aldehyde substrate for comparative assays. For inhibition studies, DIMATE (S-methyl 4-(dimethylamino)-4-methylpent-2-ynethioate) and ABD0171 (S-methyl 4-[dimethyl(2-{2,4-dimethylphenoxy}ethyl) amino]-4-methylpent-2-ynethioate) were synthesized in-house as previously described [4]. All procedures involving toxic chemicals were performed in accordance with institutional safety protocols and appropriate personal protective equipment.

2.2. Protein expression and purification

Recombinant human ALDH1A1, ALDH1A2, ALDH1A3, ALDH2 and ALDH3A1 containing an N-terminal $(His)_6$ tag were prepared following previously described protocols [1,5]. Purification involved nickel-charged agarose affinity chromatography, followed by storage at −20°C in 20 mM Tris/HCl, 500 mM NaCl, 5 mM DTT, pH 8.0.

2.3. Determination of kinetic constants

BAAA was freshly prepared by converting its precursor, BAAA-DA, from its inactive form dissolved in dimethylsulphoxide (DMSO) to BAAA through treatment with 2 M HCl. The resulting BAAA solution was subsequently diluted with ALDEFLUOR™ Assay Buffer (Fig. 1).

The absorbance spectrum of BAAA was obtained using a Cary 400 Varian UV–Visible spectrophotometer. Known concentrations of the compound were added to a final volume of 1 mL commercial Assay Buffer to determine the wavelength of maximum absorbance and calculate the molar extinction coefficient by applying the Lambert-Beer law from the linear plot of absorbance *versus* BAAA concentration. Then, the fluorescence emission spectrum of BAAA was measured in 50 mM HEPES, pH 8.0, as the routine buffer used in further experiments, using a Cary Eclipse Fluorescence spectrometer (Agilent).

The oxidation product of BAAA is the corresponding aminoacetate, which is not a commercially available compound and its fluorescence intensity is not significantly enhanced with respect to that of BAAA. Thus, NADH fluorescence was followed instead to determine the kinetic parameters of ALDH1A1, ALDH1A2, ALDH1A3 and ALDH3A1 using BAAA as a substrate. The enzymatic activity was performed in 1-mL quartz cuvettes, containing the corresponding reaction buffer for each isoform 50 mM HEPES, 0.5 mM EDTA, 0.5 mM DTT, pH 8.0, for ALDH1A1 and ALDH1A2; 50 mM HEPES, 50 mM $MgCl_2$, 5 mM DTT, pH 8.0, for ALDH1A3; and 50 mM Tris/HCl, 5 mM DTT, pH 8.0, for ALDH3A1, at 25 °C. Then, 500 μM NAD^+ for ALDH1A1, ALDH1A2 and ALDH1A3 or 1 mM $NADP^+$ for ALDH3A1, was added, and 5 μM NADH/NADPH was used as an internal standard. The reaction was initiated using different concentrations of BAAA substrate. The fluorescence of NADH/NADPH was monitored at 460 nm with excitation at 340 nm, using 10 nm for the excitation and emission spectral bandwidths [5].

A Cary 400 Varian UV–vis spectrophotometer was used to determine the absorbance spectra of MONAL-62, 6-methoxy-2-naphthoic acid (MONOIC-62), MONAL-71, 7-methoxy-1-naphthoic acid (MONOIC-71) and NADH in water:acetonitrile (60:40, v/v) for MONAL series of compounds (Fig. 2) and 50 mM HEPES, pH 8.0, for NADH. Precise substrate concentration was assessed from molar extinction coefficients for MONAL-62, $\varepsilon_{316} = 14.2 \times 10^3\ M^{-1}\ cm^{-1}$, and MONAL-71, $\varepsilon_{352} = 6.1 \times 10^3\ M^{-1}\ cm^{-1}$ [6,29]. Then, 1 μM of each compound was analyzed to

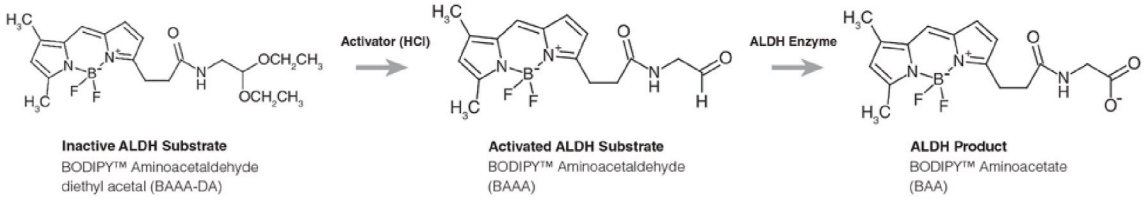

Fig. 1. Chemical structures of the inactive BAAA-DA substrate, the activated BAAA substrate, and the BAA product form of ALDEFLUOR™. Adapted from StemCell Technologies, 2011.

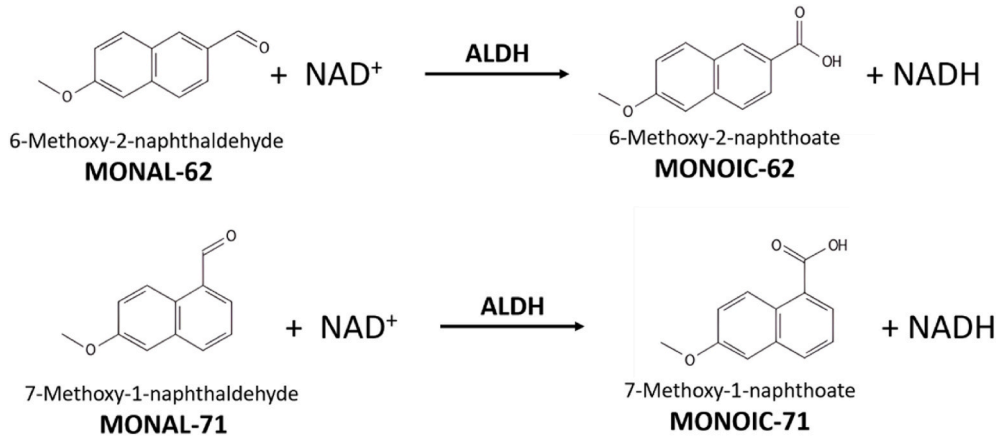

Fig. 2. Enzymatic reaction of 6-methoxy-2-naphthaldehyde (MONAL-62) and 7-methoxy-1-naphthaldehyde (MONAL-71) mediated by ALDH. In MONAL-62, the methoxy (−OCH_3) and aldehyde (−CHO) groups are both located at β positions of the aromatic naphthalene system, whereas in **MONAL-71** these groups are at α and β positions, respectively.

determine their fluorescence spectra with a Cary Eclipse fluorescence spectrometer (Agilent) when exciting at their corresponding excitation wavelength (Fig. S1). Furthermore, the fluorescence emission spectra of MONOIC-62, MONOIC-71 and NADH were also obtained when exciting at the excitation wavelength of the corresponding substrates to check for any overlapping peaks. In order to obtain the kinetic constants of ALDH1A1, ALDH1A2, ALDH1A3, ALDH2 and ALDH3A1 using MONAL series of compounds, the assays were carried out in 50 mM sodium pyrophosphate/NaOH, 0.5 mM EDTA, pH 8.1. The working solutions of substrate and internal standard were prepared freshly in reaction buffer to obtain the reaction rate at different substrate concentrations (from 0.025 to 50 μM). The assay was performed in 1-mL quartz cuvette at 37°C, adding 150 μM NAD^+ or $NADP^+$ as a cofactor. The reaction was initiated by the addition of the aldehyde substrate and the fluorescence of MONOIC-62 product was monitored at 360 nm with excitation at 288 nm, using 5 and 10 nm for the excitation and emission spectral bandwidths, respectively; the fluorescence of MONOIC-71 product was monitored at 395 nm with excitation at 331 nm, using 10 and 10 nm for the excitation and emission spectral bandwidths, respectively. Furthermore, 1 μM MONOIC-62 or MONOIC-71 was added as an internal standard to obtain the absolute reaction rate, which is calculated as described previously [5].

The enzymatic kinetic data were analyzed using GraFit 5.0 (Erithacus Software) and all data were fitted to the standard Michaelis-Menten equation. Experimental values were represented as the mean ± standard deviation from three independent measurements, while kinetic parameters were the mean ± standard error.

2.4. Molecular docking analysis

The 3D structures of ALDH1A1 (PDB code 4WB9) and ALDH1A3 (PDB codes 7QK7 and 7QK8) were used. The co-crystallized ligands, ions, and water molecules were removed from the X-ray structures and polar hydrogens were added to ensure the simulation of a biological environment by Autodock Tools [30]. The Gasteiger charges were assigned for a precise modeling of the electrostatic interactions. Then, the rotatable bonds in the MONAL series of compounds were determined and given some flexibility to improve interaction with the target. NAD^+ cofactor was adapted from ALDH1A3 structure to ALDH1A1. The processed ligands were used in a PDBQT file format. All docking calculations were carried out on the X-ray structures of human ALDH1A1 and ALDH1A3 in complex with MONAL-62 and MONAL-71, both in the presence and absence of NAD^+ cofactor. The molecular docking analysis was performed using PyRx – Phyton Prescription virtual screening software [31], which incorporates tools mainly combined from AutoDock [30] and AutoDock Vina [32]. The protein and ligands were selected in the environment associated with Vina and the binding site was defined as an inclusion region with focus located in the catalytic cysteine residue, which entirely encompassed all the binding-pocket conformations of the trajectory. The binding site was defined by a box along the x, y, and z axes centered on the catalytic cysteine (ALDH1A1: x = 21.5 Å; y = 21.0 Å; z = 22.0 Å; ALDH1A3: x = 21.0 Å; y = 21.0 Å; z = 21.0 Å). Once the grid was defined, a total of 8 models ordered according to free binding energy (ΔG) criteria and the expected pose of the ligand were generated and the top-ranked docking pose was considered as the final pose. The reliability of the docking program was assessed calculating the root-mean-square deviation (RMSD), both for lower bounds (RMSD lb) and upper bounds (RMSD ub).

2.5. Inhibition screening and determination of the IC_{50} value

Enzymatic assays were performed using single-point measurements to assess the inhibitory activity of DIMATE and ABD0171 compounds at a concentration of 10 μM against ALDH1A1 and ALDH3A1. Inhibitors were dissolved in ethanol and assayed at a final concentration of 1 % ethanol (v/v). The inhibition screening was carried out fluorometrically using a Cary Eclipse Varian fluorimeter in 50 mM sodium pyrophosphate/NaOH, 0.5 mM EDTA, pH 8.1, at 37°C, in the presence of 150 μM

NAD^+ (added after enzyme-inhibitor pre-incubation) and using a saturating concentration of substrate (5 μM MONAL-62). The effect of different pre-incubation times was also analyzed in order to study the time-dependent effect of inhibitors. Then, treatments at 5 and 20 min were tested and the remaining activity of ALDH1A1 and ALDH3A1 was obtained from the fluorescence of the reaction product MONOIC-62, which was monitored at 360 nm with excitation at 288 nm, using 5 and 10 nm for the excitation and emission spectral bandwidths. Data are presented as the mean ± standard deviation from two independent measurements using GraphPad Prism version 8.4.2 version for Windows (GraphPad Software, Boston, Massachusetts USA, www.graphpad.com).

In order to determine the IC_{50} value for ALDH1A1 with DIMATE, reaction rates were obtained at various inhibitor concentrations at a fixed saturating concentration of substrate (5 μM MONAL-62), after 5-min pre-incubation time. The IC_{50} value was calculated by non-linear fitting of the obtained data to a sigmoidal plot using GraFit 5.0 (Erithacus Software), with the following 4-parameter equation:

$$y = \frac{range}{1 + \left(\frac{x}{IC_{50}}\right)^{s}} + background$$

where y is the specific activity, x is the inhibitor concentration, *background* is the minimum y value, *range* is the fitted uninhibited value minus de background, and s is the slope factor. Experimental values were represented as the mean ± standard deviation from two independent measurements, while IC_{50} value was expressed as the mean ± standard error.

2.6. ALDH activity assays in cell extracts

Breast cancer cell lines MDA-MB-231, MDA-MB-468, and HCC70 were obtained from ATCC and cultured in DMEM, DMEM F12, or RPMI culture media, respectively, supplemented with 10 % FBS without antibiotics. Cells were maintained at 37 °C with 5 % CO_2 until reaching the exponential growth phase. Cell lysates were prepared using mammalian protein extraction reagent (M-PER, Thermo Scientific). Cell pellets were resuspended in 200 μL M-PER, lysed with two cycles of ultrasound at 110–120 V, 50–60 Hz for 5 min, and centrifuged at 16,100×*g* for 10 min at 4°C. The supernatant was collected for protein quantification. ALDH activity assays were conducted using hexanal or MONAL-62 as a substrate. In the routine method using hexanal, the reaction buffer was adapted without or with 50 mM $MgCl_2$ to set the enzymatic assay in the optimal conditions to detect ALDH1A1 or ALDH1A3 activity, as described previously [5]. Thus, 50 mM HEPES, 0.5 mM EDTA, pH 7.2, was used to detect ALDH1A1 while 50 mM HEPES, 50 mM $MgCl_2$, pH 7.2, was used to detect ALDH1A3. Enzymatic assays with 30 and 250 μM hexanal as saturating concentrations were used for ALDH1A1 and ALDH1A3, respectively. MONAL-62 assays were conducted in 50 mM sodium pyrophosphate/NaOH, 0.5 mM EDTA, pH 8.1, with 5 μM MONAL-62 as a saturating substrate concentration. Both assays were carried out at 37 °C with 500 μM NAD^+. The inhibition screening in cell extracts was carried out as described above, using 15 and 100 μM DIMATE and ABD0171. Experimental values were represented as the mean ± standard deviation from two independent measurements.

3. Results and discussion

3.1. Determination of kinetic parameters for ALDH1A isoforms using BODIPY-aminoacetaldehyde as a substrate

A comprehensive kinetic characterization of BAAA, a key substrate in the ALDEFLUOR™ assay, with each ALDH1A isoform is currently unavailable. This information is pivotal for distinguishing the roles of these isoforms in ALDH-mediated cellular processes in both healthy and diseased states. To address this gap, we conducted a detailed characterization using active recombinant human ALDH1A1, ALDH1A2, ALDH1A3, and ALDH3A1.

In order to perform the study, the spectral properties of BAAA, the ALDEFLUOR™ assay reagent, had to be determined. The UV–visible absorbance spectrum of BAAA in commercial Assay Buffer revealed a peak at 506 nm (Fig. S2). Only the spectral properties of BAAA could be characterized since the carboxylic acid form (BAA) was not commercially available. The molar extinction coefficient was calculated from the linear plot of absorbance *versus* known concentrations of the compound (Fig. S3), resulting in $\varepsilon_{506} = 33.2 \times 10^3\ M^{-1}\ cm^{-1}$. This allowed us to determine the precise substrate concentration prior to each experiment from the absorbance measurement in commercial Assay Buffer. Then, the fluorescence emission spectrum of BAAA was recorded in 50 mM HEPES, pH 8.0, as the routine buffer used in further experiments when excited at 506 nm, displaying maximum emission at 512 nm. Fluorescence emission spectrum of BAAA was also recorded by exciting at 340 nm, and no emission at 460 nm was detected (data not shown). This allowed us to follow the fluorescence of NADH/NADPH at 460 nm with excitation at 340 nm without any interference from BAAA.

Table 1 summarizes the kinetic parameters of ALDH1A isoforms using BAAA as a substrate, monitored via NADH fluorescence at 460 nm. All active isoforms displayed Michaelis-Menten kinetics with BAAA (Fig. S4). The K_m values for ALDH1A1, ALDH1A2, and ALDH1A3 were within the same micromolar range. Notably, ALDH1A2 exhibited the highest k_{cat} values, reflecting in its superior catalytic efficiency (k_{cat}/K_m = 33,500 ± 8200 $mM^{-1}\ min^{-1}$). This observation aligns with previous reports highlighting higher enzymatic rates of ALDH1A2 with various aldehyde substrates [1]. In contrast, our findings differ substantially from those previously reported by Yagishita et al. [21] for ALDH1A1, where an HPLC-based assay yielded a K_m value of 161 μM and a k_{cat} value of 465 min^{-1}. These discrepancies may arise from variations in assay conditions and detection methodologies. Additionally, consistent with previous HPLC analyses [21], ALDH3A1 exhibited negligible activity with BAAA, corroborating its limited reactivity with this substrate. These results underscore the limitations of the ALDEFLUOR™ assay in distinguishing ALDH1A isoforms, although it does not detect ALDH3A1.

3.2. Kinetic characterization of ALDH1A1, ALDH1A2, ALDH1A3, ALDH2 and ALDH3A1 isoforms using naphthaldehyde derivatives as substrates

Naphthaldehyde derivatives (MONAL-62 and MONAL-71), previously described by Wierzchowski et al.[6,29], were explored as alternative fluorescent substrates for ALDH. Here were conducted a complete kinetic characterization with five different ALDH isoforms. All active isoforms exhibited Michaelis-Menten kinetics with both MONAL-62 and MONAL-71 (Fig. S5).

ALDH1A1 demonstrated to be the most efficient enzyme for the oxidation of MONAL-62, driven by its low K_m value and a robust catalytic rate (Table 2). Conversely, ALDH1A2, despite displaying the highest k_{cat} value for MONAL-62, showed a significantly higher K_m value, resulting in a lower catalytic efficiency. ALDH1A3 exhibited the

Table 1
Kinetic constants of ALDH1A1, ALDH1A2 and ALDH1A3 with BODIPY-aminoacetaldehyde as a substrate.

Parameters	ALDH1A1	ALDH1A2	ALDH1A3	ALDH3A1
K_m (μM)	2.1 ± 0.2	5.2 ± 1.2	4.9 ± 0.7	NA
k_{cat} (min^{-1})	11.2 ± 0.4	174 ± 15	7.3 ± 0.4	NA
k_{cat}/K_m ($mM^{-1}\ min^{-1}$)	5300 ± 510	33,500 ± 8200	1500 ± 230	NA

Enzymatic activity was measured fluorometrically in the corresponding reaction buffer at 25°C. To calculate k_{cat} values, the molecular weight used was: ALDH1A1, 220,000; ALDH1A2, 226,800; and ALDH1A3, 224,000. NA, no activity was detected by using up to 30 μM BAAA and 0.3–0.8 μM enzyme. Values are the mean ± standard error.

Table 2
Kinetic constants of ALDH1A1, ALDH1A2, ALDH1A3, ALDH3A1 and ALDH2 with MONAL-62 and MONAL-71 as substrates.

Isoform	MONAL-62			MONAL-71		
	K_m (μM)	k_{cat} (min^{-1})	k_{cat}/K_m (mM^{-1} min^{-1})	K_m (μM)	k_{cat} (min^{-1})	k_{cat}/K_m (mM^{-1} min^{-1})
ALDH1A1	0.29 ± 0.09	720 ± 56	2,400,000 ± 777,300	5.08 ± 1.51	28.4 ± 2.9	56,000 ± 1755
ALDH1A2	3.50 ± 0.44	2890 ± 95	812,000 ± 103,000	8.87 ± 2.37	3.67 ± 0.34	410 ± 117
ALDH1A3	0.10 ± 0.02	4.30 ± 0.16	42,800 ± 7600	NA	NA	NA
ALDH2	1.12 ± 0.42	80 ± 6	72,000 ± 27,700	3.56 ± 1.32	0.63 ± 0.06	178 ± 68
ALDH3A1[a]	0.80 ± 0.22	1450 ± 125	1,800,000 ± 509,000	NA	NA	NA
ALDH3A1[b]	0.30 ± 0.03	270 ± 6	897,000 ± 86,000	NA	NA	NA

Enzymatic activity was measured fluorometrically at 37°C in the presence of 150 μM NAD^+ (for ALDH1 and ALDH3A1[a]) and 150 μM $NADP^+$ (for ALDH3A1[b]). To calculate k_{cat} values, the molecular weights used for ALDH1A1, ALDH1A2 and ALDH1A3 are described in Table 1, for ALDH3A1 was 100,800, and for ALDH2 was 245,000. NA, no activity was detected by using 30 μM MONAL-71 and 0.2–0.7 μM enzyme. Values were the mean ± standard error.

lowest K_m value for MONAL-62 among the active isoforms. However, its turnover rate was comparatively low, resulting in the lowest catalytic efficiency. These kinetic parameters of ALDH1A3 for MONAL-62 are characteristic of slow substrates, which typically show high affinity for the active site but a very low reaction rate.

ALDH3A1 demonstrated significant catalytic efficiency, with a k_{cat}/K_m value of 1,800,000 ± 509,000 mM^{-1} min^{-1} using NAD^+ as cofactor and 897,000 ± 86,000 mM^{-1} min^{-1} with $NADP^+$. Unlike ALDH1A isoforms, ALDH3A1 is unique in that it can utilize both $NADP^+$ and NAD^+ as cofactors [33,34]. In contrast, ALDH2 exhibited lower catalytic efficiency in oxidizing MONAL-62, reflecting a moderate K_m and a low k_{cat} value.

The ALDH isoforms generally showed minimal to no activity with MONAL-71 compared to MONAL-62 as a substrate (Table 2). Specifically, ALDH1A3 and ALDH3A1 exhibited no detectable activity. K_m values for MONAL-71 moderately increased for ALDH1A1, ALDH1A2 and ALDH2, accompanied by a substantial decrease in k_{cat} values. Notably, the k_{cat} value of ALDH1A2 decreased by three orders of magnitude, resulting in a significantly lower catalytic efficiency compared to ALDH1A1. Thus, MONAL-71 proved to be a poorer substrate than MONAL-62 across most ALDH isoforms tested, yet it remains a promising candidate for distinguishing between ALDH isoforms, particularly given the high catalytic efficiency (k_{cat}/K_m = 56,000 mM^{-1} min^{-1}) of ALDH1A1, relative to ALDH1A2 (410 mM^{-1} min^{-1}) and ALDH2 (178 mM^{-1} min^{-1}). These findings are consistent with previous reports on ALDH2, ALDH3, and unidentified isoforms of ALDH1A isolated from human tissues [6,29]. By leveraging assays that monitor MONAL-71 conversion, researchers can effectively distinguish ALDH1A1 activity from other isoforms in biochemical studies, tissue samples, or live-cell imaging scenarios where concurrent presence of other ALDH1A isoforms, as well as ALDH2 and the ALDH3 family, may occur.

Altogether, these results highlight the exquisite sensitivity of MONAL-62, which exhibits a lower detection limit of 1.95 pM ALDH1A1 (equivalent to 2 amol or 10^6 molecules of enzyme per microliter), significantly outperforming the method using hexanal based on NADH fluorescence (detection limit of 140 pM enzyme). The superior sensitivity of MONAL-62 can be attributed to the higher quantum yield of MONOIC-62 compared to that of NADH (Table S1) and the higher k_{cat} value (720 min^{-1}) of ALDH1A1 for MONAL-62 relative to hexanal (31 min^{-1}). Conversely, for ALDH1A3, MONAL-62 offers lower sensitivity with detection limit of 1380 pM enzyme, whereas hexanal affords a lower limit of 70 pM ALDH1A3, further underscoring the selectivity of MONAL-62 for ALDH1A1 over ALDH1A3. This selective capability of MONAL-62 proves advantageous in biological samples with low ALDH activity, enabling enhanced discrimination between ALDH isoforms. The identification of ALDH1A1 would be further enhanced by combining the use of MONAL-71 as a substrate, which is not active with ALDH1A3 and shows low activity with ALDH1A2.

3.3. Molecular docking analysis of naphthaldehyde derivatives reveals isoform-specific interactions with ALDH1A1 and ALDH1A3

Molecular simulations were employed to elucidate the distinct kinetic behavior observed between ALDH1A1 and ALDH1A3 when interacting with naphthaldehyde derivatives. These isoforms were selected due to their structural similarity within the ALDH1A subfamily, yet they exhibit markedly different kinetic properties with the naphthaldehyde derivatives. The simulations aimed to rationalize these divergent kinetic profiles, shedding light on the underlying molecular interactions that govern substrate specificity and catalytic efficiency in ALDH enzymes. The molecular docking analysis of MONAL-62 and MONAL-71 with ALDH1A1 and ALDH1A3 isoforms revealed significant differences in substrate orientation and interaction with the active-site residues (Figs. 3 and 4).

Regarding the interaction between MONAL-62 and ALDH1A1, the carbonyl group of the substrate adopted a favorable orientation towards the active-site cysteine residue (Cys303, Fig. 3A). Despite appearing distant from the NAD^+ cofactor, the Y-shaped orientation facilitated electron transfer and efficient catalysis. Additionally, the substrate was stabilized through aromatic interactions, forming a face-to-face (RING FF) interaction with Phe171 and an offset face-to-face (RING OF) interaction with both Phe171 and Tyr297. This strong stabilization suggests that the larger atomic volume of the catalytic pocket in ALDH1A1 allows for conformational flexibility, potentially enhancing catalytic rates through structural rearrangements within the active site. The low ΔG and RMSD values correlated well with low K_m values, indicating strong enzyme-substrate binding and optimal positioning within the active site. This minimal conformational fluctuation of MONAL-62 upon binding suggested precise alignment of its reactive functional groups, facilitating favorable transition state formation and reducing the energetic barrier for the enzymatic reaction.

MONAL-62 exhibited a stronger binding affinity with ALDH1A3, supported by its slightly more favorable ΔG and lower RMSD values (Fig. 3B). Moreover, the stability of MONAL-62 within ALDH1A3 active site was supported by multiple interactions with aromatic residues, such as Phe182, which engaged in RING FF interactions at a close distance of 3.2 Å. Additionally, Phe182 formed RING OF interactions with the adjacent aromatic ring of the naphthalene system, with minor edge-to-edge interactions (RING EE) also involving Phe308 and the naphthalene ring. This latter interaction, although weaker, contributed to substrate stabilization necessary for the catalytic reaction mediated by Cys314. While the distance between the nucleophilic residue and the carbonyl carbon of MONAL-62 was 4.2 Å, the NAD^+ cofactor was positioned optimally at 4.7 Å for the reaction. Despite strong substrate binding, the conversion of MONAL-62 into product may occur at a relatively slow rate, consistent with the low k_{cat} value of ALDH1A3 (Table 2). This could be due to an extended residence time of the substrate within the narrower active site pocket of ALDH1A3, where multiple stabilizing interactions formed a tightly bound complex, potentially hindering the conformational changes required for efficient catalytic turnover. This characteristic resembled that of the inhibitor

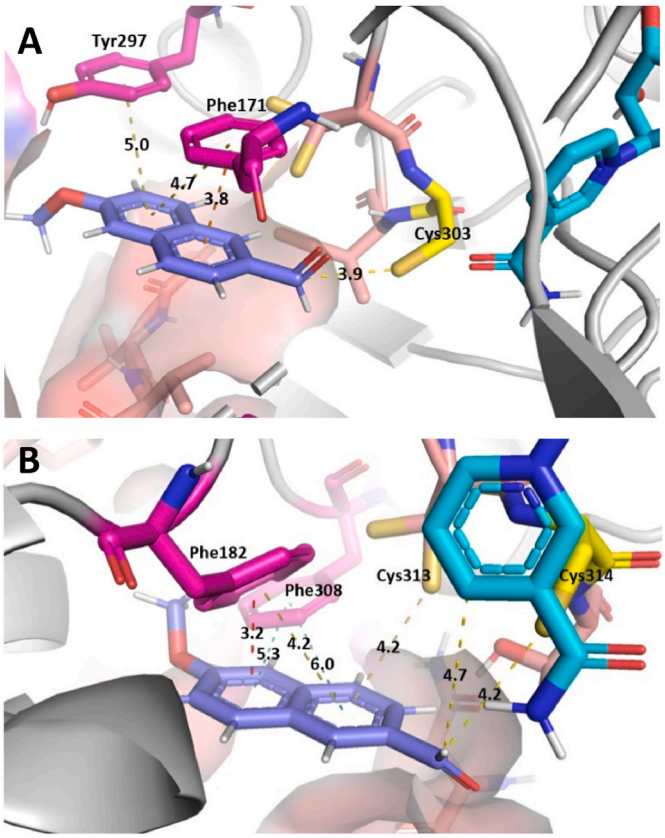

Fig. 3. Molecular docking analysis of MONAL-62 with ALDH1A1 and ALDH1A3 isoforms. A) Docking of MONAL-62 with ALDH1A1 (ΔG = −7.0 kcal/mol; RMSD lb = 1.361 Å; RMSD ub = 5.391 Å). π-π stacking (RING OF type) interactions are observed between the two rings of the ligand and Phe171 and Tyr297, along with a RING FF interaction with Phe171. These stabilizing interactions enable the substrate to be ideally positioned near Cys303, suggesting an optimal configuration for a high-rate reaction, potentially correlating with an increased k_{cat} value. **B)** Docking results of MONAL-62 with ALDH1A3 (ΔG = −7.4 kcal/mol; RMSD lb = 0.927; RMSD ub = 2.391). Multiple π-π stacking (RING FF and RING OF type) interactions are observed between the two rings of the ligand and Phe182, along with additional RING EE interactions with Phe308. These interactions contribute to the stabilization of the substrate, positioning the carbonyl carbon atom at 4.2 Å from Cys314.

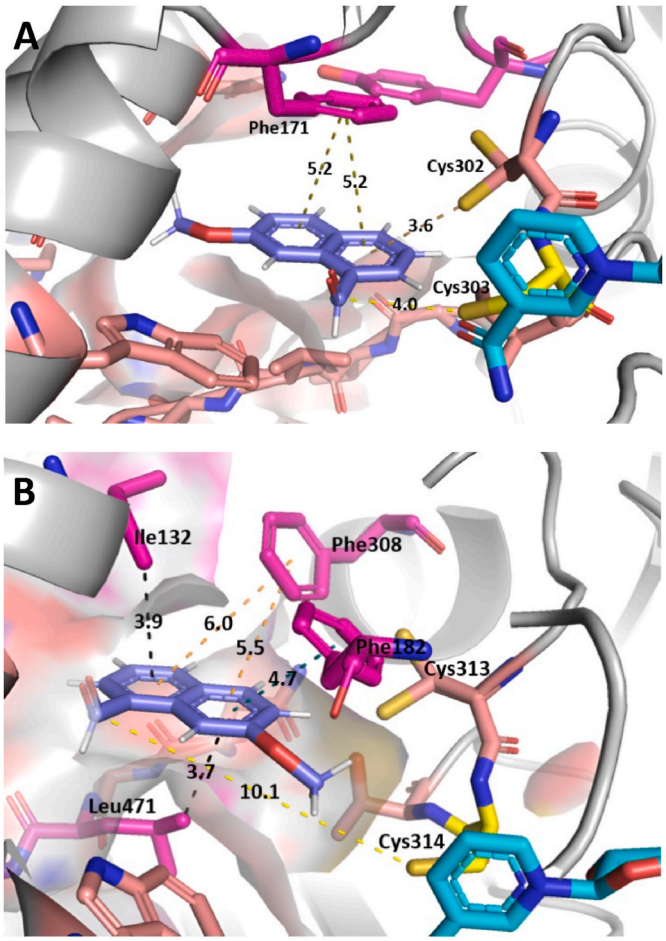

Fig. 4. Molecular docking analysis of MONAL-71 with ALDH1A1 and ALDH1A3 isoforms. A) Docking of MONAL-71 with ALDH1A1 (ΔG = −6.9 kcal/mol; RMSD lb = 1.999; RMSD ub = 3.402). In this case, the substrate successfully reaches the catalytic site near Cys303, suggesting a favorable environment for the enzymatic reaction. The substrate is stabilized by π-π (RING OF) interactions with Phe171 and a sulphur-π interaction with Cys302, ensuring optimal orientation for catalysis. **B)** Docking of MONAL-71 with ALDH1A3 (ΔG = −6.4 kcal/mol; RMSD lb = 2.491; RMSD ub = 4.282). The inhibitor is sequestered at the entrance of the active site due to interactions with Ile132 and Leu471 through carbon-π interactions. Additionally, π-π stacking (RING OT and RING EF) interactions with Phe182 and Phe308 further stabilize the inhibitor at this location. As a result, MONAL-71 is unable to reach the catalytic Cys314, preventing the enzymatic reaction.

diethylaminobenzaldehyde (DEAB) [35], suggesting that MONAL-62 acts as a slow substrate for ALDH1A3.

Fig. 4 depicts MONAL-71 interactions with ALDH1A1 and ALDH1A3. In ALDH1A1, MONAL-71 was optimally docked to the catalytic site, interacting primarily with Cys303 at a productive atomic distance of 4 Å, and stabilized through RING OF interactions with Phe171 and a sulphur-π interaction with Cys302 (Fig. 4A). Conversely, in ALDH1A3, the carbonyl group of MONAL-71 was improperly oriented because the molecule was stacked at the active site entrance, due to extensive interactions with key residues such as Ile132 and Leu471 (Fig. 4B). These were primarily carbon-**π** interactions, which were more significant than typical aromatic interactions, also present. Specifically, Phe182 facilitated offset-stacked (RING OT) interactions, while Phe308 generated edge-to-face (RING EF) interactions. These stabilizations resulted in non-productive substrate binding, since the distance between the carbonyl carbon of MONAL-71 and Cys314 exceeded 10 Å despite a favorable binding energy.

These differences reflect the larger active-site pocket of ALDH1A1 [1], facilitating better substrate orientation and reducing steric hindrance for enzymatic reaction. Structural differences between MONAL-71 and MONAL-62 further highlight how the position of methoxy and carbonyl groups in the aromatic ring of MONAL-71 may cause steric clashes in ALDH1A3, hindering correct aldehyde positioning, while the orientation of functional groups in MONAL-62 enables better accommodation within the active site.

Noteworthy, structural predictions from molecular docking analyses were in good agreement with the experimental kinetic results. Particularly, the more favorable and productive binding of MONAL-62 and MONAL-71 to ALDH1A1 over ALDH1A3 accounts for the higher enzymatic activity of ALDH1A1 with these naphthalene derivatives. Overall, these findings underscore how active site topology and ligand structural orientation influence substrate binding and enzymatic activity in the ALDH1A1 and ALDH1A3 isoforms.

3.4. Selective inhibition of ALDH1A1 by DIMATE: A tool for discriminating ALDH isoform activities in biological samples

DIMATE and its analogue, ABD0171, are emerging enzymatic inhibitors currently advancing through clinical and preclinical research stages, respectively, and demonstrating distinct inhibitory profiles

against different ALDH isoforms. DIMATE and ABD0171 preferentially target ALDH1A isoforms, showing promising selective inhibition. Once ALDH1A1 was identified as one of the most active isoforms with MONAL-62 (Table 2), an IC_{50} assay was conducted to determine the concentration range of DIMATE required for complete inhibition of MONAL-62 oxidation by ALDH1A1 (Fig. 5). Establishing this threshold is essential for optimizing the use of DIMATE as a selective inhibitor, ensuring effective targeting of ALDH1A1 while minimizing potential off-target effects.

The use of MONAL-62 as a substrate in the IC_{50} assay of ALDH1A1 with DIMATE offered two main advantages: 1) an enhanced fluorescent signal due to the higher quantum yield of its carboxylic acid product as compared to NADH; 2) a greater inhibitory effect of DIMATE compared to when hexanal was used as a substrate. With a pre-incubation time of 5 min, the IC_{50} value of ALDH1A1 for DIMATE with MONAL-62 was 9.2 ± 2.8 μM, which is significantly lower than 37 ± 5 μM, observed with hexanal even after 20-min pre-incubation [4]. This difference could be attributed to the bulkier nature of MONAL-62, which may further restrict substrate access to the enzyme active site in the presence of inhibitor. Similar effects towards lower IC_{50} values had been observed with larger substrates such as all-*trans*-retinaldehyde compared to hexanal [4]. The combination of improved fluorescence detection and increased inhibition efficiency highlights the advantages of MONAL-62 in assessing ALDH1A1 activity and the potency of selective inhibitors like DIMATE.

The enzymatic activity of ALDH1A1 and ALDH3A1, using MONAL-62 as a substrate, was assessed to evaluate the selective inhibitory effect of DIMATE and ABD0171, after 5- and 20-min pre-incubation times (Fig. 6). The results demonstrate the potential of DIMATE as a selective inhibitor against ALDH1A1 and its high effectiveness in discriminating between ALDH1A1 and ALDH3A1. DIMATE significantly reduced the enzymatic activity of ALDH1A1 for both 5- and 20-min pre-incubation periods, with a more pronounced inhibitory effect observed after 20 min. This confirms that DIMATE inhibition against ALDH1A1 is time dependent, consistent with previous reports [4]. In contrast, the inhibitory effect of DIMATE on ALDH3A1 was less pronounced and not time-dependent, indicating that DIMATE exerts stronger inhibitory

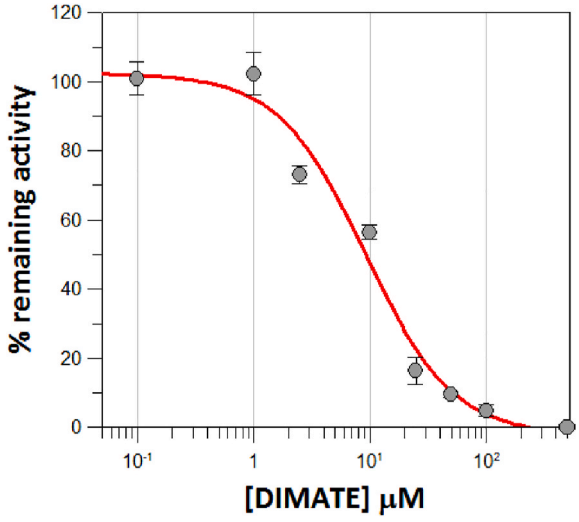

Fig. 5. Sigmoidal representation to calculate the IC_{50} value of ALDH1A1 with DIMATE. The percentage of remaining activity is plotted against the logarithm of inhibitor concentration. Enzymatic activity was measured fluorometrically at 37°C in 50 mM pyrophosphate/NaOH, 0.5 mM EDTA, pH 8.1. NAD^+ concentration was 500 μM and the substrate was 5 μM MONAL-62 (saturating concentration). The pre-incubation time was 5 min in the absence of cofactor, internal standard and substrate. Data are presented as the mean ± standard deviation from duplicate measurements and the IC_{50} value (9.2 ± 2.8 μM) is shown as the mean ± standard error.

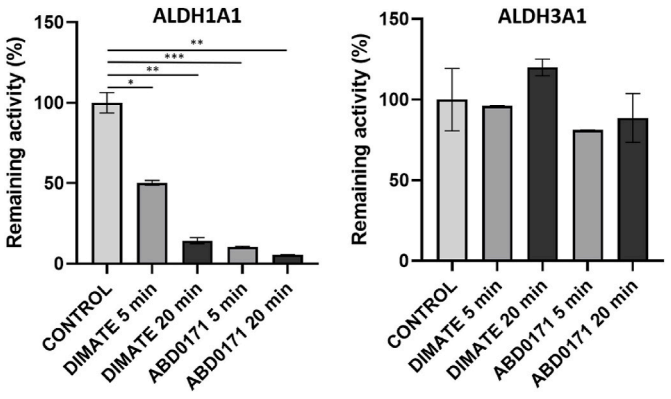

Fig. 6. Enzymatic activity of ALDH1A1 and ALDH3A1 with MONAL-62 in the presence of DIMATE and ABD0171 with 5- and 20-min pre-incubation. Enzymatic activity was measured fluorometrically in 50 mM sodium pyrophosphate/NaOH, 0.5 mM EDTA, pH 8.1, at 37°C, in the presence of 150 μM NAD^+ and using 5 μM MONAL-62. Inhibitor concentration was 10 μM DIMATE and ABD0171. Fluorescence of the reaction product MONOIC-62 was monitored at 360 nm with excitation at 288 nm. Data are presented as the mean ± standard deviation from duplicate measurements.

action on ALDH1A1 relative to ALDH3A1. Similar results were obtained with a DIMATE analogue, ABD0171, which displayed an even greater inhibitory effect. These results also reproduce the increased selectivity of these inhibitors against ALDH1A1 as compared to ALDH3A1 [4]. The selective inhibition of ALDH1A1 is particularly valuable for distinguishing between these isoforms in complex biological samples where both may be present. By using DIMATE or ABD0171, researchers can effectively suppress ALDH1A1 activity without significantly affecting ALDH3A1, allowing for a more accurate identification and measurement of ALDH3A1 activity. This ability to selectively inhibit ALDH1A1 while preserving ALDH3A1 function is crucial for studies that aim to differentiate between these isoforms and investigate their specific roles in various biological processes. Therefore, DIMATE and ABD0171 serve as essential tools for exploring isoform-specific functions of ALDH enzymes, enhancing our understanding of their contributions to cellular metabolism and pathophysiology in different biological contexts.

3.5. The use of MONAL-62 as a substrate along with inhibitors enable complete ALDH1A1 inhibition in triple-negative breast cancer cell lines

Breast cancer MDA-MB-231, MDA-MB-468, and HCC70 cells typically express multiple ALDH isoforms, prominently ALDH1A1 and ALDH1A3, along with high levels of ALDH2 and ALDH3A1 [4]. ALDH activity in these cell lines has been previously assessed by using the ALDEFLUOR™ method focusing on ALDH1A1 and ALDH1A3 contributions [16,17]. In the present study, we measured the endogenous ALDH activity in cell extracts by using the routine substrate hexanal, adapted for ALDH1A1 (without Mg^{2+}) and ALDH1A3 (with Mg^{2+}), alongside with MONAL-62. Comparable ALDH activity values (1.42–2.80 mU/mg) were obtained across all cell lines using hexanal (Table 3). Under ALDH1A3 conditions, activity levels for the three cell extracts were consistently higher than those for ALDH1A1.

Incubation with DIMATE and ABD0171 inhibitors revealed significant but incomplete inhibition of ALDH activity in all three cell lines, indicating their effect primarily on inhibitor-sensitive isoforms (mainly ALDH1A). The most substantial inhibitory effect was observed in HCC70 cells, where DIMATE reduced activity to 41.8 and 47.5 % for ALDH1A1 and ALDH1A3, respectively, while ABD0171 reduced activity to 39.4 and 42.7 % for ALDH1A1 and ALDH1A3, respectively.

Alternatively, we measured ALDH activity in cell extracts using MONAL-62 as a substrate, yielding similar values in MDA-MB-231 and HCC70 cells (0.72 and 0.87 mU/mg, respectively) but much lower in

Table 3
Inhibition of ALDH1 enzymatic activity in MDA-MB-231, MDA-MB-468, and HCC70 cell extracts following incubation with DIMATE and ABD0171, using hexanal as a substrate.

Cell line	ALDH1A1[a]					ALDH1A3[b]				
	Control Activity (mU/mg)	DIMATE	ABD0171	DIMATE	ABD0171	Control Activity (mU/mg)	DIMATE	ABD0171	DIMATE	ABD0171
		15 μM		100 μM			15 μM		100 μM	
		Remaining activity (%)					Remaining activity (%)			
MDA-MB-231	1.77 ± 0.12	77.7 ± 7.4	60.4 ± 16.6	63.5 ± 1.7	80.0 ± 11.8	2.80 ± 0.21	74.4 ± 5.4	90.1 ± 7.4	61.0 ± 7.8	67.7 ± 11.8
MDA-MB-468	1.42 ± 0.15	77.9 ± 6.1	82.5 ± 6.1	59.9 ± 5.4	63.1 ± 5.8	2.07 ± 0.24	76.3 ± 7.5	73.4 ± 3.7	45.2 ± 3.8	42.4 ± 5.3
HCC70	1.63 ± 0.16	86.0 ± 10.9	55.6 ± 6.3	41.8 ± 2.5	39.4 ± 2.1	2.56 ± 0.13	64.5 ± 13.5	67.8 ± 10.9	47.5 ± 9.8	42.7 ± 0.6

The remaining enzymatic activity was measured fluorometrically using hexanal as a substrate under saturating conditions (30 μM and 250 μM for ALDH1A1 and ALDH1A3, respectively). The reaction mixture was pre-incubated for 20 min at 37°C in the presence of 15 and 100 μM DIMATE or ABD0171, in the following assay mixture: [a]For ALDH1A1, 50 mM HEPES, 0.5 mM EDTA, pH 7.2. [b]For ALDH1A3, 50 mM HEPES, 50 mM $MgCl_2$, pH 7.2. After pre-incubation, 500 μM NAD^+, 5 μM NADH as an internal standard and hexanal were added. Data are reported as the percentage of remaining enzymatic activity with respect to the untreated control. Experimental values are the mean ± standard deviation.

MDA-MB-468 cells ($^{0.025\pm0.001}$ mU/mg). In the former two cell lines, activity values were comparable to those measured with hexanal as a substrate (Table 3). The lower activity detected in MDA-MB-468 cells suggests a different isoform profile with reduced expression of MONAL-62-specific isoforms (likely ALDH1A1 and ALDH3A1). Incubation with 100 μM DIMATE or ABD0171 resulted in complete inhibition of the enzymatic activity when MONAL-62 was used as a substrate, indicating effective targeting of ALDH1A isoforms. Therefore, the combination of MONAL-62, which is more isoform specific than hexanal, along with inhibition by DIMATE and ABD0171, improves our ability to characterize the isoform composition of complex low-activity cell extracts.

4. Conclusions

ALDH is increasingly used as a biomarker in cancer tumors, which show a wide heterogeneity regarding isoform composition. Existing models to assess ALDH activity, such as the ALDEFLUOR™ assay, lack sufficient discrimination among different ALDH isoforms. In addition, a comprehensive kinetic characterization with BAAA, the ALDEFLUOR™ substrate, had not been previously conducted. This work study achieves a comprehensive characterization of ALDH isoforms using BAAA, by monitoring the fluorescence emission of NADH at 460 nm. BAAA proved effective across all ALDH1A isoforms, with K_m values in the micromolar range (2.1–5.2 μM). ALDH1A2 displayed the highest k_{cat} value (174 min^{-1}) while ALDH3A1 demonstrated no activity with BAAA consistent with previous findings. As an alternative approach for assessing ALDH activity in cellular extracts, we explored MONAL-62 and MONAL-71 as fluorogenic substrates and the kinetic constants of ALDH isoforms were determined. MONAL-62 offered exquisite sensitivity with a detection limit as low as 1.95 pM ALDH1A1, significantly surpassing the routine assay with hexanal in selectivity and sensitivity. Combined with selective ALDH1A inhibitors, such as DIMATE and ABD0171, the MONAL-62 assay proved to be an invaluable tool for quantifying ALDH1A1 activity in complex biological samples, even in the presence of other isoforms. Furthermore, the high substrate specificity of ALDH1A1 for MONAL-71 provides an additional assay for the unambiguous identification of this isoform. This method successfully detected ALDH1A isoform activity in extracts from triple-negative breast cancer. In conclusion, the adoption of the MONAL-62/MONAL-71 assays represents a significant advancement in the detection of ALDH1A1, addressing the limitations of hexanal-based assays and offering enhanced precision and reliability in both research and clinical applications.

CRediT authorship contribution statement

Raquel Pequerul: Writing – review & editing, Writing – original draft, Validation, Methodology, Investigation, Formal analysis, Data curation, Conceptualization. **Daniela Covaleda:** Methodology, Investigation, Formal analysis, Data curation. **Andrés S. Sánchez-Vaca:** Methodology, Investigation, Formal analysis, Data curation. **Laura Torres:** Methodology, Investigation. **Andrada Constantinescu:** Methodology, Investigation, Formal analysis, Data curation. **Mileidys Perez-Alea:** Writing – review & editing, Supervision, Investigation, Formal analysis, Data curation, Conceptualization. **Xavier Parés:** Writing – review & editing, Supervision, Conceptualization. **Jaume Farrés:** Writing – review & editing, Writing – original draft, Validation, Supervision, Project administration, Funding acquisition, Formal analysis, Data curation, Conceptualization.

Declaration of competing interest

MP is a shareholder in Advanced BioDesign. The remaining authors declare no conflicts of interest.

Acknowledgements

This research was partially funded by the Spanish Ministerio de Ciencia, Innovación y Universidades (Agencia Estatal de Investigación, grant numbers PID2020-119424RB-I00/AEI/10.13039/501100011033 and PID2023-150696NB-I00/MCIU/AEI/10.13039/501100011033/FEDER, UE). This research was also supported by the Agència de Gestió d'Ajuts Universitaris i de Recerca (AGAUR, grup consolidat N-TETRASCAN 2021SGR00135). RP obtained financial support from the company Advanced BioDesign through a research contract agreement with Universitat Autònoma de Barcelona. AC was supported by a doctoral PhD fellowship under the program Plan France Relance 2024 (CRISPALDHin). We are indebted to Dr. Marina Corbella (Universitat de Barcelona) who validated the molecular docking analyses, and Dr. Salvador Bartolomé and the Servei de Genòmica i Espectroscòpia de Biomolècules (SGiEB) for providing access to the Cary Eclipse fluorescence spectrometers (Agilent). We would like to dedicate this work to Kai Martínez Pequerul and Rai Carbonell Farrés, who have been a constant source of inspiration and joy during the preparation of this manuscript.

Appendix A. Supplementary data

Supplementary data to this article can be found online at https://doi.org/10.1016/j.cbi.2025.111609.

Data availability

Data will be made available on request.

References

[1] R. Pequerul, J. Vera, J. Giménez-Dejoz, I. Crespo, J. Coines, S. Porté, C. Rovira, X. Parés, J. Farrés, Structural and kinetic features of aldehyde dehydrogenase 1A (ALDH1A) subfamily members, cancer stem cell markers active in retinoic acid biosynthesis, Arch. Biochem. Biophys. 681 (2020), https://doi.org/10.1016/j.abb.2020.108256.

[2] M. Rhinn, P. Dollé, Retinoic acid signalling during development, Development 139 (2012) 843–858, https://doi.org/10.1242/dev.065938.

[3] P. Marcato, C.A. Dean, C.A. Giacomantonio, P.W.K. Lee, Aldehyde dehydrogenase its role as a cancer stem cell marker comes down to the specific isoform, Cell Cycle 10 (2011) 1378–1384, https://doi.org/10.4161/cc.10.9.15486.

[4] R. Pequerul, A. Constantinescu, B. Janji, A. Kumar, X. Parés, O. Palacios, D. Colignon, A. Berrou, G. Fournet, P. Berchard, G. Martin, I. Ceylan, R. Rebollido-Ríos, J. Farrés, M. Perez-Alea, ALDH1 subtype-specific inhibitor targets key cancerous epithelial cell populations in aggressive subtypes of breast cancer, bioRxiv (2024), https://doi.org/10.1101/2024.10.18.619128.

[5] R. Pequerul, S. Porté, X. Parés, M. Pérez-Alea, J. Farrés, Production, purification, and fluorometric activity assay of human aldehyde dehydrogenases, Bio Protoc. 12 (2022), https://doi.org/10.21769/BioProtoc.4505.

[6] J. Wierzchowski, E. Interewicz, P. Wroczynski, I. Orlanska, Continuous fluorimetric assay for human aldehyde dehydrogenase and its application to blood analysis, Anal. Chim. Acta 319 (1996) 209–219, https://doi.org/10.1016/0003-2670(95)00476-9.

[7] P. Wroczyns Ki, J. Wierzchowski, J. Golab, M. Blazejczyk, D. Borecka, Determination of aldehyde dehydrogenase (ALDH) isozymes in human cancer samples-comparison of kinetic and immunochemical assays, Molecules 7 (2002) 896–901, https://doi.org/10.3390/71200896.

[8] K. Orywal, W. Jelski, T. Werel, M. Szmitkowski, The diagnostic significance of serum alcohol dehydrogenase isoenzymes and aldehyde dehydrogenase activity in urinary bladder cancer patients, Anticancer Res. 37 (2017) 3537–3541, https://doi.org/10.21873/anticanreS.11722.

[9] K. Orywal, W. Jelski, T. Werel, M. Szmitkowski, The diagnostic significance of serum alcohol dehydrogenase isoenzymes and aldehyde dehydrogenase activity in prostate cancer patients, Anticancer Res. 37 (2017) 4961–4965, https://doi.org/10.21873/anticanres.11906.

[10] K. Orywal, W. Jelski, T. Werel, M. Szmitkowski, The activity of class I, II, III and IV alcohol dehydrogenase isoenzymes and aldehyde dehydrogenase in renal cell carcinoma, Exp. Mol. Pathol. 98 (2015) 403–406, https://doi.org/10.1016/j.yexmp.2015.03.012.

[11] K. Orywal, W. Jelski, T. Werel, M. Szmitkowski, The alterations in alcohol dehydrogenase and aldehyde dehydrogenase activities in the sera of patients with renal cell carcinoma, Adv. Med. Sci. 63 (2018) 1–4, https://doi.org/10.1016/j.advms.2017.05.001.

[12] K. Orywal, W. Jelski, T. Werel, M. Szmitkowski, The activity of class I-IV alcohol dehydrogenase isoenzymes and aldehyde dehydrogenase in bladder cancer cells, Cancer Invest. 36 (2018) 66–72, https://doi.org/10.1080/07357907.2017.1422511.

[13] S. Michorowska, A. Wiśniewska, R. Wolinowska, P. Wroczyński, J. Giebułtowicz, The applicability and limitations of the spectrofluorometric method for determination of ALDH1 activity in serum and plasma, Diagnostics 14 (2024), https://doi.org/10.3390/diagnostics14232721.

[14] R.W. Storms, A.P. Trujillo, J.B. Springer, L. Shah, O. Michael Colvin, S. M. Ludeman, C. Smith, Isolation of primitive human hematopoietic progenitors on the basis of aldehyde dehydrogenase activity, Cell Biol. 96 (1999) 9118–9123, https://doi.org/10.1073/pnas.96.16.9118.

[15] J.S. Moreb, D. Ucar, S. Han, J.K. Amory, A.S. Goldstein, B. Ostmark, L.J. Chang, The enzymatic activity of human aldehyde dehydrogenases 1A2 and 2 (ALDH1A2 and ALDH2) is detected by aldefluor, inhibited by diethylaminobenzaldehyde and has significant effects on cell proliferation and drug resistance, Chem. Biol. Interact. 195 (2012) 52–60, https://doi.org/10.1016/j.cbi.2011.10.007.

[16] L. Zhou, D. Sheng, D. Wang, W. Ma, Q. Deng, L. Deng, S. Liu, Identification of cancer-type specific expression patterns for active aldehyde dehydrogenase (ALDH) isoforms in ALDEFLUOR assay, Cell Biol. Toxicol. 35 (2019) 161–177, https://doi.org/10.1007/s10565-018-9444-y.

[17] J.J. Duan, J. Cai, L. Gao, S.C. Yu, ALDEFLUOR activity, ALDH isoforms, and their clinical significance in cancers, J. Enzym. Inhib. Med. Chem. 38 (2023), https://doi.org/10.1080/14756366.2023.2166035.

[18] C. Anorma, J. Hedhli, T.E. Bearrood, N.W. Pino, S.H. Gardner, H. Inaba, P. Zhang, Y. Li, D. Feng, S.E. Dibrell, K.A. Kilian, L.W. Dobrucki, T.M. Fan, J. Chan, Surveillance of cancer stem cell plasticity using an isoform-selective fluorescent probe for aldehyde dehydrogenase 1A1, ACS Cent. Sci. 4 (2018) 1045–1055, https://doi.org/10.1021/acscentsci.8b00313.

[19] I. Minn, H. Wang, R.C. Mease, Y. Byun, X. Yang, J. Wang, S.D. Leach, M.G. Pomper, A red-shifted fluorescent substrate for aldehyde dehydrogenase, Nat. Commun. 5 (2014), https://doi.org/10.1038/ncomms4662.

[20] T.E. Bearrood, G. Aguirre-Figueroa, J. Chan, Rational design of a red fluorescent sensor for ALDH1A1 displaying enhanced cellular uptake and reactivity, Bioconjug. Chem. 31 (2020) 224–228, https://doi.org/10.1021/acs.bioconjchem.9b00723.

[21] A. Yagishita, T. Ueno, H. Esumi, H. Saya, K. Kaneko, K. Tsuchihara, Y. Urano, Development of highly selective fluorescent probe enabling flow-cytometric isolation of ALDH3A1-Positive viable cells, Bioconjug. Chem. 28 (2017) 302–306, https://doi.org/10.1021/acs.bioconjchem.6b00618.

[22] A. Yagishita, T. Ueno, K. Tsuchihara, Y. Urano, Amino BODIPY-based blue fluorescent probes for aldehyde dehydrogenase 1-Expressing cells, Bioconjug. Chem. 32 (2021) 234–238, https://doi.org/10.1021/acs.bioconjchem.0c00565.

[23] M. Oe, K. Suzuki, K. Miki, H. Mu, K. Ohe, Steric control in activator-induced nucleophilic quencher detachment-based probes: high-contrast imaging of aldehyde dehydrogenase 1A1 in cancer stem cells, Chempluschem 87 (2022), https://doi.org/10.1002/cplu.202200319.

[24] M. Oe, K. Miki, Y. Ueda, Y. Mori, A. Okamoto, Y. Funakoshi, H. Minami, K. Ohe, Deep-red/near-infrared Turn-On fluorescence probes for aldehyde dehydrogenase 1A1 in cancer stem cells, ACS Sens. 6 (2021) 3320–3329, https://doi.org/10.1021/acssensors.1c01136.

[25] A. Okamoto, Y. Funakoshi, M. Oe, R. Takai, H. Suto, Y. Nagatani, M. Nishimura, Y. Imamura, T. Kunihisa, N. Kiyota, K. Miki, K. Ohe, H. Tanino, H. Minami, Identification of breast cancer stem cells using a newly developed long-acting fluorescence probe, C5S-A, targeting ALDH1A1, Anticancer Res. 42 (2022) 1199–1205, https://doi.org/10.21873/anticanres.15586.

[26] Q. Wang, Z. Li, Y. Hao, Y. Zhang, C. Zhang, Near-infrared fluorescence probe with a new recognition moiety for specific detection and imaging of aldehyde dehydrogenase expecting the identification and isolation of cancer stem cells, Anal. Chem. 94 (2022) 17328–17333, https://doi.org/10.1021/acs.analchem.2c04801.

[27] S. Ghosh, S. Ghosh, A. Majee, S. SenGupta, S. Mukherjee, B. Roy, R. Das, A. Mukherjee, A fluorogenic probe for screening and kinetic evaluation of aldehyde dehydrogenase 1A1 (ALDH1A1) inhibitors, ChemRxiv (2025), https://doi.org/10.26434/chemrxiv-2025-h4q1t.

[28] J.W. Park, K.H. Jung, Y. Byun, J.H. Lee, S.H. Moon, Y.S. Cho, K.H. Lee, ATP-Binding cassette transporters substantially reduce estimates of ALDH-Positive cancer cells based on aldefluor and AldeRed588 assays, Sci. Rep. 9 (2019), https://doi.org/10.1038/s41598-019-42954-9.

[29] J. Wierzchowski, P. Wroczynski, K. Laszuk, E. Interewicz, Fluorimetric detection of aldehyde dehydrogenase activity in human blood, saliva, and organ biopsies and kinetic differentiation between class I and class III isozymes, Anal. Biochem. 245 (1997) 69–78, https://doi.org/10.1006/abio.1996.9921.

[30] D.S. Goodsell, M.F. Sanner, A.J. Olson, S. Forli, The AutoDock suite at 30, Protein Sci. 30 (2021) 31–43, https://doi.org/10.1002/pro.3934.

[31] S. Dallakyan, A.J. Olson, C.C. Hong, Small-molecule library screening by docking with PyRx. https://doi.org/10.1007/978-1-4939-2269-7_19, 2015.

[32] J. Eberhardt, D. Santos-Martins, A.F. Tillack, S. Forli, AutoDock vina 1.2.0: new docking methods, expanded force field, and python bindings, J. Chem. Inf. Model. 61 (2021) 3891–3898, https://doi.org/10.1021/acs.jcim.1c00203.

[33] J. Perozich, I. Kuo, B.C. Wang, J.S. Boesch, R. Lindahl, J. Hempel, Shifting the NAD/NADP preference in class 3 aldehyde dehydrogenase, Eur. J. Biochem. 267 (2000) 6197–6203, https://doi.org/10.1046/j.1432-1327.2000.01697.x.

[34] A. Pappa, T. Estey, R. Manzer, D. Brown, V. Vasiliou, Human aldehyde dehydrogenase 3A1 (ALDH3A1): biochemical characterization and immunohistochemical localization in the cornea, Biochem. J. 376 (2003) 615–623, https://doi.org/10.1042/BJ20030810.

[35] C.A. Morgan, B. Parajuli, C.D. Buchman, K. Dria, T.D. Hurley, N,N-diethylaminobenzaldehyde (DEAB) as a substrate and mechanism-based inhibitor for human ALDH isoenzymes, Chem. Biol. Interact. 234 (2015) 18–28, https://doi.org/10.1016/j.cbi.2014.12.008.